OXFORD SIMB Society for Industrial Microbiology and Biotechnology

Journal of Industrial Microbiology and Biotechnology, 2025, 52, kuaf006

https://doi.org/10.1093/jimb/kuaf006
Advance access publication date: 26 February 2025
Environmental Microbiology – Original Paper

Metagenomic mining unveils a novel GH130 enzyme with exclusive xylanase activity over a wide temperature and pH ranges

Amr A. Hemeda[1], Sara A. Zahran[1], Marwa Ali-Tammam[1], Menna A. Ewida[2], Mona T. Kashef[3], Aymen S. Yassin[3], Avishek Mitra[4], Noha H. Youssef[4], Mostafa S. Elshahed[4]

[1]Department of Microbiology and Immunology, Faculty of Pharmacy, Future University in Egypt, 12311 Cairo, Egypt
[2]Department of Pharmaceutical Chemistry, Faculty of Pharmacy, Future University in Egypt, 12311 Cairo, Egypt
[3]Department of Microbiology and Immunology, Faculty of Pharmacy, Cairo University, Cairo 11562, Egypt
[4]Department of Microbiology and Molecular Genetics, Oklahoma State University, Stillwater, OK 74074, USA
Correspondence should be addressed to: Marwa Ali-Tammam at marwa.ali@fue.edu.eg and Mostafa S. Elshahed at Mostafa@okstate.edu

Abstract: The equine gut harbors a diverse microbial community and represents a rich source of carbohydrate-active enzymes (CAZymes). To identify and characterize potentially novel CAZymes from a horse's hindgut metagenome, shotgun metagenomic sequencing was performed on DNA extracted from a stool sample of a male horse, followed by CAZyme annotation. Here, we report on the characterization of a novel enzyme (AH2) that was identified, synthesized, cloned, and characterized from the obtained CAZyme dataset. AH2 was identified as a GH130 family member and displayed exclusive xylanase activity, a trait hitherto unreported in prior characterization of GH130 CAZymes. AH2 displayed an optimal activity at a pH of 5.6 and a temperature of 50°C. AH2 maintained significant activity across a pH range of 4–10 (62–72%) and temperatures of 30–70°C (77–86%). The enzyme had remarkable stability, with minimal reductions in activity across a temperature range of 4–70°C and pH levels of 3, 7, and 9. Docking studies identified AH2's amino acids (Glu90 and Glu149) to be involved in substrate binding. Molecular dynamics simulation confirmed the structural stability of AH2 at pH 5.6 and 50°C, further supporting its resilience under these conditions. Our results expand on the known activities associated with the GH130 CAZyme family and demonstrate that the horse gut metagenome represents an unexplored source of novel CAZymes.

One-Sentence Summary: A novel activity for members of the CAZyme family GH130.

Keywords: Carbohydrate-active enzymes (cazymes), Equine hindgut, Glycoside hydrolases (GHs), Xylanase

Graphical abstract

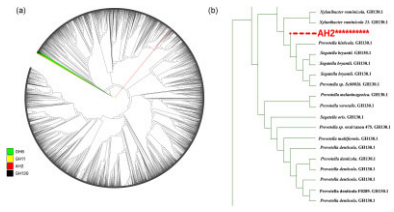

Introduction

Mammalian herbivores employ different strategies for effective degradation of plant cell biomass (Bergmann, 2017). The majority of mammalian herbivores are either foregut fermenters, possessing a specialized stomach chamber (rumen), or hindgut fermenters, possessing an enlarged caecum. Within these specialized rumen or caecum chambers, a highly diverse microbial community develops and secretes a diverse array of carbohydrate-degrading enzymes (carbohydrate-active enzymes [CAZymes]), such as endoglucanases, exoglucanases, beta-glucosidases, xylanases, and lignin peroxidases, that efficiently convert animal feed into short-chain volatile fatty acids, a major nutrient source for the host animal (Takizawa et al., 2020).

Previous studies have predominantly focused on the microbial community of ruminants like cattle and sheep. Unlike ruminants, horses are hindgut fermenters, relying more extensively on the microbial population residing in their hindgut for fermentation and digestion (Karasov & Douglas, 2013; Dicks et al., 2014; Stewart et al., 2018; Cholewińska et al., 2020; Forcina et al., 2022). Horse's diet includes a substantial amount of plant polymers such as cellulose, hemicelluloses, and pectins, ranging from 35 to 60%. Such polymers are resistant to digestion by the horse's own enzymes, necessitating the involvement of hindgut microbial enzymes in their breakdown (Julliand & Grimm, 2017). Recently, Li and colleagues have suggested that most CAZymes in the equine gut are currently unexplored (Li et al., 2023).

Received: September 24, 2024. **Accepted:** February 25, 2025.

Therefore, the horse's hindgut represents a poorly explored fermentation system hosting potent lignocellulolytic microbes encoding different novel CAZymes, facilitating the conversion of lignocellulosic feed mainly into volatile fatty acids, an essential step for equine life.

Carbohydrate active enzymes (CAZymes) is a collective term that encompasses all enzymes involved in the synthesis or breakdown of polysaccharides. According to the CAZy database (Drula et al., 2022), CAZymes are classified into six main classes: glycoside hydrolases (GHs), glycosyl transferases (GTs), polysaccharide lyases, carbohydrate esterases (CEs), carbohydrate-binding modules, and auxiliary activities. These enzymes cleave glycosidic linkages, release sugars and ultimately facilitate nutrient absorption by the host herbivore. CAZymes have traditionally been identified in sequenced genomes of various (micro)organisms. Recently, direct identification and characterization of CAZymes in metagenomic datasets have widely been implemented to circumvent the need for isolation and access the CAZyme repertoires of yet-uncultured and difficult to culture microbial taxa (Berlemont & Martiny, 2015).

In this study, we aimed to identify novel CAZymes in a horse hindgut metagenomics dataset. We report on a GH130 family enzyme harboring xylanase-activity, deviating from the primary enzymatic activity conventionally attributed to this family. The discovered enzyme was active and stable over a wide range of pH and temperatures and encodes the conserved residues necessary for xylan degradation.

Materials and Methods

Sample Collection and DNA Extraction

A fresh stool sample was collected from an adult male domestic horse approximately 5 years, in Helwan district, Cairo, Egypt. The sample was immediately placed in a sterile 50-mL plastic tube post-defecation, sealed, and transported to the laboratory on ice within an hour (Meili et al., 2023). Upon arrival, the sample was stored at −20°C until DNA extraction. DNA was extracted using the DNeasy Plant Pro Kit (Qiagen®, Germantown, MD), following the manufacturer's guidelines.

Shotgun Metagenomic Sequencing and Assembly

Shotgun metagenomic sequencing was performed using NextSeq 2 K P2 2 × 300-bp paired-end technology, with standard library preparation using the IDT XGen library kit. Sequencing was conducted at the University of Oklahoma, Clinical Genomics Facility. Subsequent read processing and assembly were executed using the KBase online server (Arkin et al., 2018). Briefly, Illumina adapter sequences were removed using BBTools v38.22, and high-quality reads were retained using Trimmomatic v.0.36 with a sliding window size of 4 and a minimum quality of 15 (Bolger et al., 2014). To achieve an assembly of high-quality reads, various software tools were employed, including MegaHit v1.2.9 (using both meta-large and meta-sensitive assembly (Li et al., 2015), IDBA-UD—v1.1.3 (Peng et al., 2012), Velvet Assembler—v1.2.10 (Zerbino & Birney, 2008), and metaSPAdes—v3.15.3 (Nurk et al., 2017). These tools were set with a minimum kmer of 27, maximum kmer of 127, and a minimum contig length of 1 000 bp. Subsequently, the selection of the best assembly was based on a comprehensive comparison using Compare Assembled Contig Distributions—v1.1.2 (Wu et al., 2016). The assembly with the most optimal component contig lengths and size distribution was chosen.

CAZyme Annotation and Selection Criteria

CAZyme gene-containing contigs within the best assembly were annotated using the dbCAN2 meta server for automated CAZyme annotation (Zhang et al., 2018), applying both HMMER (Potter et al., 2018) and DIAMOND (Buchfink et al., 2021) tools with default settings. Alignments with less than 60% identity were discarded to enhance precision and reduce false positive findings (Rost, 1999). Identified CAZymes were organized based on their similarity score, and those with a similarity between 80 and 90% were validated using BLASTX (O'Leary et al., 2016) against the non-redundant protein database (nr) of the National Center for Biotechnology Information (NCBI), NCBI's conserved domain database (Marchler-Bauer et al., 2015), Pfam (Mistry et al., 2021), and InterPro (Mitchell et al., 2015).

Synthesis and Cloning of Putative Enzyme-Encoding Gene

The gene encoding the selected putative enzyme, designated as AH2, with a length of 1176 bp, was synthesized for expression in *Escherichia coli*. This gene was synthesized and inserted into a pET-21a(+) plasmid using the services of a commercial provider (GenScript, Piscataway, NJ). *Escherichia coli* DH5α (Thermo Fisher, Waltham, MA) was utilized for plasmid propagation, while *E. coli* BL21(DE3) (Invitrogen, Carlsbad, CA) served as an expression host. The recombinant plasmid containing the gene of interest was introduced into *E. coli* BL21(DE3) cells via heat-shock transformation (Froger & Hall, 2007) and the transformed cells were selected by overnight incubation at 37°C on pre-dried LB agar plates containing 100 μg/mL of ampicillin.

Gene Expression and Enzyme Purification

Escherichia coli BL21(DE3) cells transformed with the recombinant plasmid were grown in LB broth supplemented with ampicillin (100 μg/mL) at 37°C with agitation at 200 rpm until reaching an optical density of 0.6 at 600 nm. Induction of protein expression was achieved by adding isopropyl ß-D-1-thiogalactopyranoside to a final concentration of 1 mM, followed by further incubation at 37°C for 1, 2, and 3 hrs. Cells were harvested by centrifugation at 5000× *g* for 5 min. The harvested cell pellets were resuspended in phosphate-buffered saline (pH 7.4) containing 1 mM phenylmethylsulfonyl fluoride and subjected to sonication (40% amplitude, and 30 sec on/off cycle pulses) until the tubes became transparent (Sankey et al., 2023). Whole-cell lysates were obtained by centrifugation at 1 500× *g* for 20 min at 4°C.

Enzyme purification was carried out by affinity chromatography, using Ni-NTA Agarose resin (Thermo Fisher Scientific, St. Louis, MO, USA), according to the manufacturer's protocol. Crude extract and purified enzyme were analyzed by sodium dodecyl sulfate-polyacrylamide gel electrophoresis (SDS-PAGE; Laemmli, 1970). Imidazole was removed using Slide-A-Lyzer Dialysis Cassettes (Thermo Fisher, Waltham, WA), against imidazole-free phosphate-buffered saline (Makowska-Grzyska et al., 2014). Protein concentration was determined using the Bicinchoninic acid (BCA) Protein Assay Kit (Thermo Fisher Scientific), following the manufacturer's instructions.

Enzyme Assays

The endoglucanase, exoglucanase, xylanase, and mannanase activities of the purified enzyme were assessed using carboxymethyl cellulose sodium salt (1.25% w/v), avicel microcrystallinecellulose (1.25% w/v), beechwood xylan (1.25% w/v), and locust bean gum (0.5% w/v) as substrates, respectively (all obtained from

Sigma-Aldrich, Waltham, MA, USA). Enzyme assays were performed at 50°C for 20 min in 50 mM sodium acetate buffer (pH 5.6) (Morrison et al., 2016). Following the reaction, the quantification of the produced reducing sugars was determined using the 3,5-dinitrosalicyclic acid method (Breuil & Saddler, 1985). Standard curves were constructed using glucose, xylose, or mannose. All experiments were conducted in duplicates. The enzymatic activity was quantified in units (U), where one unit of activity represents the amount of enzyme that releases one micromole of reducing sugar equivalents per minute. The specific activity was computed by assessing the units released per milligram of enzyme (Watzlawick, 2017).

Effect of pH on Enzyme Activity and Stability

The influence of pH on the activity and stability of AH2 was examined across a range of pH values. The enzymatic activity was assessed, as previously described, at pH of 3, 4, 5.6, 7, 8, 9, and 10 using the following buffer systems: sodium acetate (50 mM, pH 3–6), sodium phosphate (50 mM, pH 7), tris–HCl (50 mM, pH 8–9), and glycine-NaOH (50 mM, pH 10) (Xiang et al., 2019). Relative activities were reported as a fraction of the maximum activity under optimal conditions. The stability of AH2 under different pH conditions was evaluated by incubating 100 μL of the purified enzyme at pH of 3, 5.6, 7, 9, and 11 (using glycine-NaOH buffer for pH 11) for 1 hr at 4°C (Morrison et al., 2016). Following incubation, the residual enzymatic activity was determined by the 3,5-dinitrosalicyclic acid assay (Breuil & Saddler, 1985) and the relative activity was calculated by comparison to the untreated enzyme. All experiments were conducted in duplicate.

Effect of Temperature on Enzyme Activity and Stability

The enzymatic activity was evaluated across a temperature range from 30 to 80°C, with 10°C intervals, and the activity was calculated relative to that of the enzyme with maximum activity. To evaluate the thermal stability, the purified enzyme was incubated for 1 hr at different temperatures; 4, 25, 37, 50, and 70°C. Following incubation, the tubes were rapidly cooled in an ice bath, and the residual enzyme activity was assayed. The relative activity was determined by comparing the enzyme activity of the treated samples with that of the untreated enzyme. All experiments were conducted in duplicate.

Sequence Homology and Phylogenetic Analysis

The sequence homology and phylogenetic relationships between AH2 and publicly available GH130 proteins were analyzed. A comprehensive search of the CAZy database via the dbCAN3 platform (http://dbcan.unl.edu/dbcan/), last updated on August 13, 2024, identified 4 864 sequences belonging to the GH130 family from a total of 3 613 704 sequences. The dataset was manually curated to exclude GeneCatalog_proteins (hypothetical proteins), resulting in a refined dataset of 4 786 sequences, which was used for phylogenetic analysis. To further explore AH2's evolutionary relationships, sequences from the GH8 and GH11 families—both known for their xylanase activity—were included, allowing for a comparative analysis of AH2's positioning relative to other xylanase-active GH enzymes. Multiple Sequence Comparison by Log-Expectation (MUSCLE) (Madeira et al., 2022) was conducted using Mega 11 software (Molecular Evolutionary Genetics Analysis), with default settings (Tamura et al., 2021). The phylogenetic tree was generated by adopting the maximum-likelihood method with an estimated proportion of invariable sites and bootstrapping with 1 000 replicates as implemented in FastTree v.2 (Price et al., 2010). The generated phylogenetic tree was visualized and annotated using the Interactive Tree of Life web-based tool, facilitating an unbiased exploration of sequence-based classification.

In Silico Prediction of AH2-Xylan Interaction

To elucidate the interaction between AH2 and xylan, seven different crystal structures of proteins with endo-β-1,4-xylanase activity [PDB IDs: 1B30 (Gübitz, 1999), 1B31 (Gübitz, 1999), 1AXK (Aÿ et al., 1998)], β-1,3-xylosidase [PDB IDs: 1PX8 (Yang et al., 2004), 1W91], and endo-1,3-β-xylanase [PDB IDs: 2DDX (Agarwal et al., 2011; Sakaguchi et al., 2011), 3VPL (Zhao et al., 2023)] were subjected to molecular docking to pinpoint regions of significant sequence similarity. Discovery Studio 4.1 Software was utilized for molecular docking simulations (Cantarel et al., 2009; Nin-Hill et al., 2023). Additionally, a homology model of AH2 was constructed using the crystal structure of a homologous protein (PDB ID: 3WAS) identified through a BLAST search of the Protein Data Bank (http://www.rcsb.org/pdb). The 3WAS template was selected due to its favorable structural alignment and validation in terms of secondary and tertiary structure. The AH2 sequence was aligned with the 3WAS template using a multiple-sequence alignment protocol, and the resulting 3D model was generated based on this alignment. Structural evaluation of the model revealed a sequence identity of approximately 79.43% and a sequence similarity of 100% with the template, confirming the reliability of the generated structure.

Molecular Docking of Macromolecules

The crystal structures of the seven xylanase proteins were downloaded from the Protein Data Bank (www.rcsb.org) and prepared for protein alignments. The proteins were subjected to cleaning procedures, including the addition of hydrogen atoms to amino acid residues to complete missing residues, water molecules were removed, and a Force Field approach using CHARMm and MMFF94 partial charges was applied. The seven sequences of β-xylanases were subjected to superimposition and protein alignment with AH2. RMSD (Root mean square deviation) was studied as a measure of the average distance between the atoms of superimposed protein structures.

Molecular Docking of Small Molecule Ligand to AH2

The small molecule ligand co-crystallized with the protein 1B31, the xylanase protein with the best alignment result to AH2, was prepared for molecular modelling simulation study via the "Prepare Ligand" protocol; Force Field using CHARMm and MMFF94 partial charge was applied. Docking the ligand into the binding site of AH2 was performed using the C-DOCKER algorithm. The resulting binding modes were studied to confirm the biological activity along with the binding affinity of AH2 (Elhusseiny et al., 2022).

Molecular Dynamics (MD) Simulation

The Molecular Dynamics Simulation (MD simulation) was employed to validate the stability of AH2. The AH2-ligand complex was enrolled to the MD simulation using Discovery Studio 4.1. client. CHARMm force field parameters for the investigated protein were generated automatically. The protein residue was adjusted to standard ionization states at normal physiological conditions (pH 7.0). Finally, the MD simulations were run for 200 ns under constant pressure (NVT ensemble). Data calculation

Table 1. Family Classification of Predicted CAZymes in the Horse Metagenome Sample using DIAMOND

Class	GH	GT	CBM	PL	CE	Total
Subjects	296	114	81	3	20	514
Families	50	16	50	2	16	134

Note. GH = glycoside hydrolases; GT = glycoside transferases; CBM = carbohydrate-binding modules; PL = polysaccharide lyases; CE = carbohydrate esterases.

includes calculation of the binding free energy, RMSD and root-mean-square fluctuation (RMSF) to predict the stability of the studied protein. The stability of AH2 was investigated over a temperature range of 290–370 K (16.85–96.85°C) and a pH range of 4.9–6.8.

Nucleotide Sequence Accession Number

Shotgun metagenomics sequences have been deposited in GenBank under BioProject number PRJNA887424, BioSample: SAMN34141582; Sample name: Horse_168; SRA: SRS17292849. The sequence of AH2 xylanase extracted from this metagenomic sample is provided in the supplementary document and has been deposited in GenBank under accession number PQ389436.

Results

Almost 1.96 Gbp raw sequence data from 13 071 068 reads were obtained. Among various assemblies available through Kbase, MegaHit provided the best output (highest N50, highest number of Contigs >100 Kb) and was used for subsequent CAZyme prediction.

CAZymes Prediction and Sequence Analysis

A total of 514 CAZymes-encoding genes (with ≥60% identity) were predicted. The identified CAZyme belonged to 134 different families from the MegaHit assembly file, according to the DIAMOND tool. The class of GHs was the most abundant, identifying 296 candidates across 50 families (Table 1).

Bottom of Form

DIAMOND annotation output was used for a subsequent filtration process, applying a similarity threshold of 80–90%, ensuring the discovery of novel variants while retaining conserved regions and aiding in exploring functional variation. This resulted in the identification of 21 CAZymes, including 12 GHs, four GTs, and one CE, along with four proteins displaying multiple identities (Supplementary Table S1). Focusing specifically on GHs (the most abundant class), a putative enzyme from the GH130 family, AH2 (ORF ID: k141_99 292_3), was selected with 86.3% similarity (Supplementary Fig. S1).

Cloning, Expression, and Purification of AH2 Enzyme

The recombinant plasmid containing AH2 gene inserts was transformed into *E. coli* BL21 (DE3), as an expression host. The expression analysis revealed a distinct band corresponding to the expected product size of AH2 of approximately 45 kDa (computed using the Compute pI/Mw tool; https://web.expasy.org/compute_pi/). Purification of AH2 through nickel affinity chromatography was assessed via SDS-PAGE analysis, where AH2 was mainly detectable in the 500 mM imidazole elute fraction (Fig. 1).

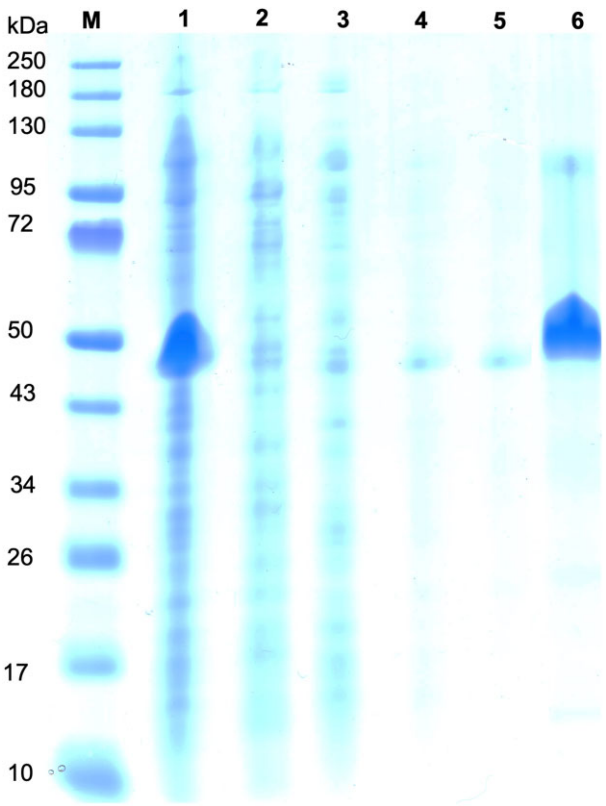

Fig. 1. AH2 purification by nickel affinity chromatography. SDS-PAGE visualization of proteins from whole cell lysate (Lane 1), the flow through (Lane 2), first wash with 20 mM imidazole (Lane 3), second wash with 30 mM imidazole (Lane 4), third wash with 40 mM imidazole (Lane 5), and purified AH2 eluted with 500 mM imidazole (Lane 6). The gel highlights the successful purification of AH2 protein using nickel affinity chromatography. M = protein molecular weight marker.

Enzymatic Characterization of AH2 Enzyme Activity

The potential endoglucanase, exoglucanase, xylanase, and mannanase activities of AH2 were assessed. Interestingly, AH2 only exhibited xylanase activity with a specific activity of 5.5 ± 0.28 U/mg at 50°C and pH 5.6. No detectable endoglucanase, exoglucanase, or mannanase activities were observed above the levels of the negative control under the stated experimental conditions. It is interesting to note that characterized members of the GH130 family primarily exhibit mannoside phosphorylase and mannosidase activities (Li et al., 2020). To date, no xylanase activity has been reported to the best of our knowledge.

Effect of pH on enzyme activity and stability

The pH dependency of AH2 xylanase activity was investigated using different buffers over a pH range of 3–10. Optimal enzyme activity was observed at pH 5.6. Activities were detected between pHs 3 and 10, with relatively high activity levels (62–72% of the optimal activity from 4 to 10 (Fig. 2a).

AH2 demonstrated maximum stability at pH 5.6, with minimal reductions in stability observed at pH 3, 7, and 9 (with residual enzymatic activity of 75.46 ± 5.63, 81.33 ± 7.65, 82.85 ± 1.74%, respectively). Exposure to extreme alkaline conditions, at pH 11, resulted in reduced residual activity (32.06 ± 6.99%; Fig. 2b).

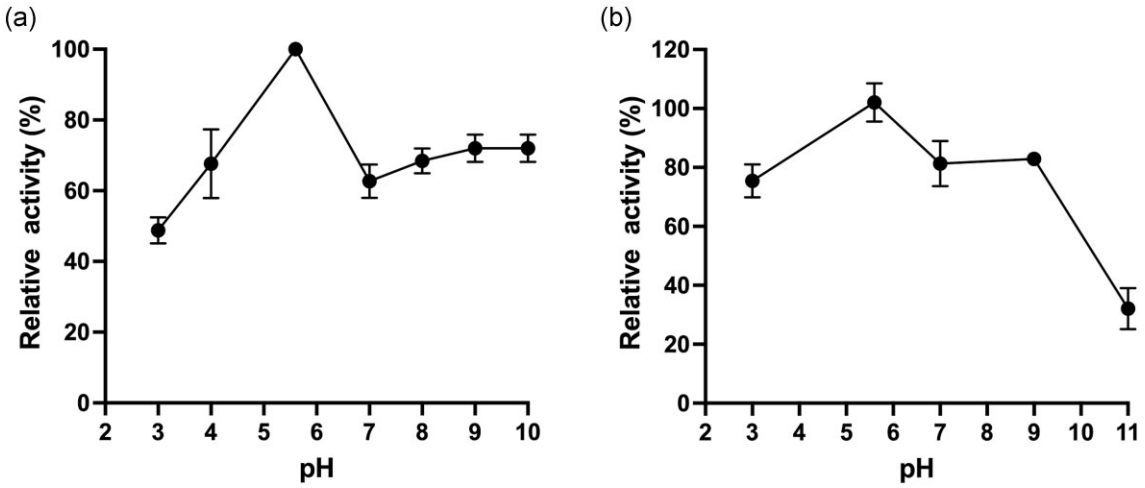

Fig. 2. Effect of pH on AH2 xylanase (a) activity and (b) stability. Enzymatic activity was measured at 50°C for 20 min in different buffer systems with different pH; sodium acetate (pH = 3, 4, and 5.6), sodium phosphate (pH = 7), tris–HCl (pH = 8 and 9), and glycine-NaOH (pH = 10). pH stability was determined by incubating the enzyme at various pH levels of 3, 5.6, 7, 9, and 11 (using glycine-NaOH buffer at pH = 11) for 1 hr at 4°C. Results are presented as the mean of duplicates ± standard deviation, represented by error bars.

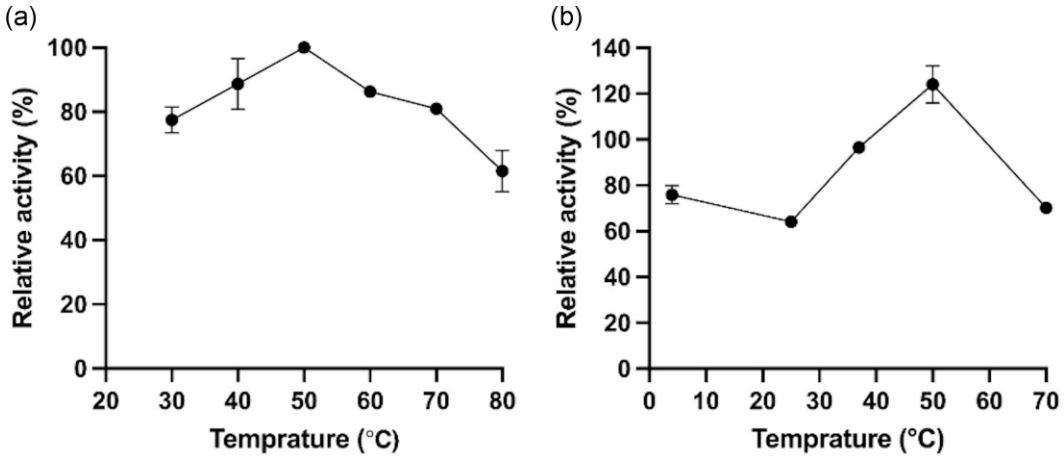

Fig. 3. Effect of temperature on AH2 xylanase (a) activity and (b) stability. Xylanase activity was assayed at different temperatures between 30 and 80°C with intervals of 10°C. Thermostability was determined by incubating the enzyme at 4, 25, 37, 50, and 70°C for 1 hr. Results are presented as the mean of duplicates ± standard deviation, represented by error bars.

Effect of temperature on enzyme activity and stability

The highest xylanase activity of AH2 was observed at 50°C. Remarkably, minimal reductions in activity were recorded at temperatures of 30–70°C, ranging from 77.49 ± 4.04% to 86.32 ± 0.58%. However, a notable decrease occurred at 80°C, resulting in approximately 61.7 ± 6.37% of the maximum observed activity (Fig. 3a). In addition, the thermostability of AH2 was assessed across a spectrum of temperatures ranging from 25 to 70°C, along with an additional assessment at 4°C (Fig. 3b). At 4, 37, and 70°C, the enzyme exhibited 75.90 ± 3.99, 96.57 ± 1.04, and 70.16 ± 2.42% of its residual activity, respectively. At room temperature (25°C), AH2 maintained considerable stability (64.16 ± 1.21% residual activity). Moreover, incubation at 50°C for 1 hr enhanced the enzyme's activity.

Phylogenetic Analysis

The phylogenetic tree reveals that AH2 (highlighted in red) clusters with a well-supported group of GH130 enzymes (in black), underscoring its significant sequence similarity within the GH130 family. However, the marked phylogenetic distance between AH2 and the GH8 (green) and GH11 (yellow) families—both appeared as outgroups and are known for their xylanase activity—highlights that, despite AH2's functional similarity in terms of xylanase activity, it exhibits considerable sequence divergence from these established xylanase-active families. The closest relatives to AH2 within the GH130 family are five GHs derived from *Segatella* (previously known as *Prevotella*). Notably, one of these enzymes, AGH13967.1, originating from a *Prevotella* species found in the bovine rumen, has demonstrated endoglucanase and mannanase activities. However, it exhibits no activity against other polysaccharides such as xylan, xyloglucan, and lichenan (Fig. 4) (Rosewarne et al., 2014). An overview analysis of the taxonomic distribution of GH130 enzyme-producing bacteria at the phylum and genus levels reveals that the phylum Bacteroidota is the most prevalent, comprising nearly 31% of GH130 producers. This is followed by Bacillota at approximately 13% and Pseudomonadota at around 7%. At the genus level, *Bacteroides* is the most prominent, accounting for about 15% of GH130 producers, with *Paenibacillus* next at roughly 8%.

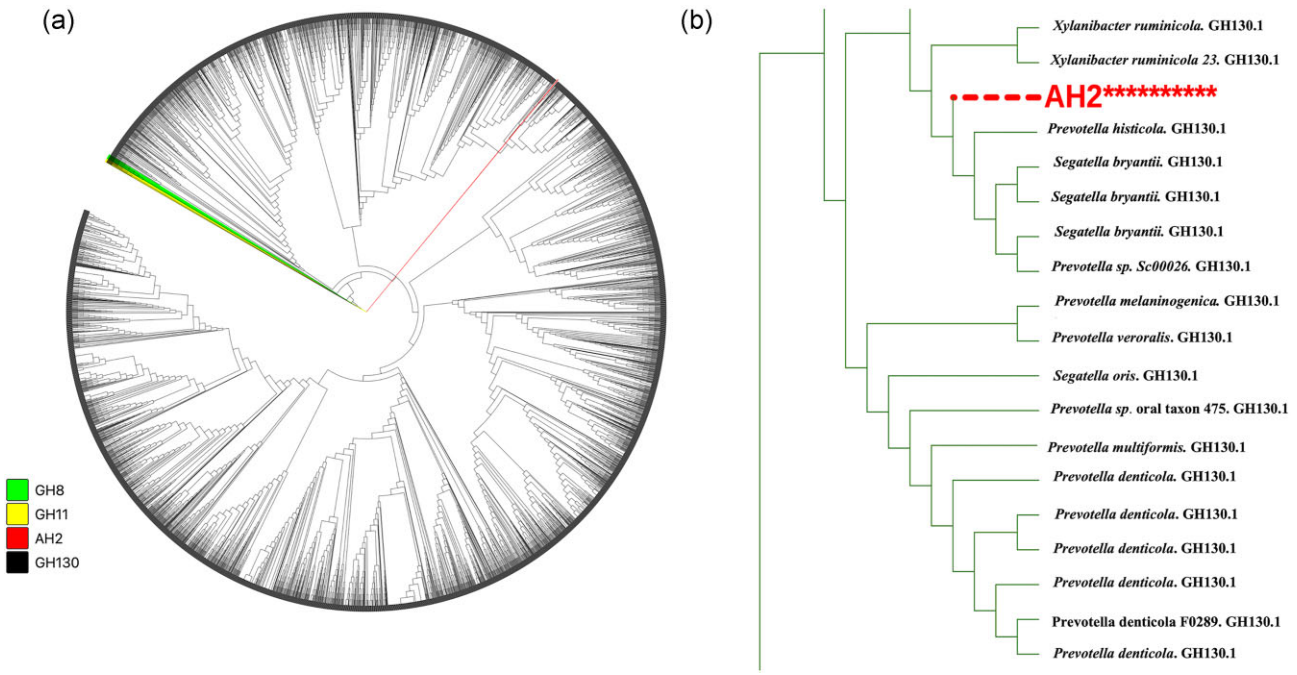

Fig. 4. Phylogenetic analysis of AH2 and GH130 family sequences. (a) Circular maximum likelihood phylogenetic tree illustrating the evolutionary relationships between AH2 and other GH130 family sequences. Distinct clustering within GH130 reflects evolutionary divergence, with AH2 positioned in a well-supported clade, indicating close relationships with other GH130 enzymes. GH8 and GH11, appeared as outgroups, demonstrate clear divergence from the GH130 lineage. (b) A section of the rectangular phylogenetic tree highlights AH2's proximity to its closest relatives from *Segatella* (formerly *Prevotella*). The figure was prepared using ITOL, and phylogenetic distances were computed under the JTT model (FastTree). Branch lengths are relative and not to scale.

Alignments and Docking of AH2

The AH2 protein from the homology modeling was superimposed and aligned with seven different xylanase enzymes (Supplementary Table S2). The superimposition results demonstrated significant alignment between AH2 and each of these xylanase enzymes, indicating strong conservation of structural features across the compared sequences. The alignment and superimposition of AH2 (yellow) with β-1,4-xylanase 1B31 (blue) shared the least RMSD (19.772 Å) along with the greatest number of conserved residues involved in ligand binding: Glu56-Asn58-Gln75-Lys79-Asn131 of 1B31 with Asn69-Asn73-Glu90-Arg94-Glu149 of AH2 (Fig. 5a, b).

Molecular Docking of AH2 to the Small Molecule Ligand

The docking of AH2 to the small molecule ligand co-crystallized with β-1,4-xylanase 1B31 (beta-D-xylopyranose-(1–4)-beta-D-xylopyranose) was performed. The 2D-diagram of the docking analysis revealed AH2-substrate interaction energy within a favorable range of −43.58 to −53.048 kcal/mol. Notably, the reported substrate consistently formed hydrogen bonds with specific amino acid residues in the AH2 binding pocket. These residues included Arg94, Arg88, Glu149, and Asp343. Additionally, Van der Waals interactions were observed between the substrate and residues Arg94, Val318, and Asp343. These interactions contribute to the overall binding affinity and specificity between the substrates and AH2 (Fig. 6).

Molecular dynamics simulations were utilized to explore the dynamic behavior of the AH2 protein, extending the analysis beyond the static insights provided by molecular docking. RMSD analysis demonstrated that the AH2 protein maintained a stable backbone conformation (Fig. 7a). Additional support for its stability was found through RMSF analysis (Fig. 7b), where the low RMSF values (<4 Å for most residues) indicated the inherent stability of the AH2 protein. The energy profile (Fig. 8a) showed an average energy range of −13 200 to −13 320 kcal/mol, further confirming the protein's stability. The stability of the protein was evaluated over a temperature range of 290–370 K (16.85–96.85°C), where system temperature was below 330 K (56.85°C) most of the time (Fig. 8b). Additionally, a pH stability assessment was conducted within the range of 4.9—6.8 to validate the protein's stability at pH 5.6. (Fig. 8c).

Discussion

We here report on a novel enzyme, AH2, exhibiting an exclusive xylanase activity and belonging to GH130. Currently (August 2024), the CAZy database lists 5 246 GH130 enzymes, of which only 20 are characterized. Seventeen are mannoside phosphorylase and three are mannosidase. Reporting xylanase activity in GH130 is significant, since to the best of our knowledge, no prior similar activity in this family has been reported. Members of the GH130 family primarily demonstrate mannoside phosphorylase activity, targeting β-1,2- and β-1,4-mannosidic linkages (Macdonald et al., 2019; Li et al., 2020). Notably, Nihira et al. (2015) identified a GH130 enzyme from *Dyadobacter fermentans*, which exhibited no synthetic activity with α-D-mannose 1-phosphate but instead released α-D-mannose from β-1,2-mannooligosaccharides with inversion of the anomeric configuration, classifying it as a β-1,2-mannosidase. Similarly, a β-1,2-mannosidase from *Bacteroides thetaiotaomicron* is capable of hydrolyzing macromolecular mannan (Cuskin et al., 2015). These findings illustrate the structural and functional versatility of GH130 enzymes but suggest that their activity has primarily been confined to mannoside-related substrates.

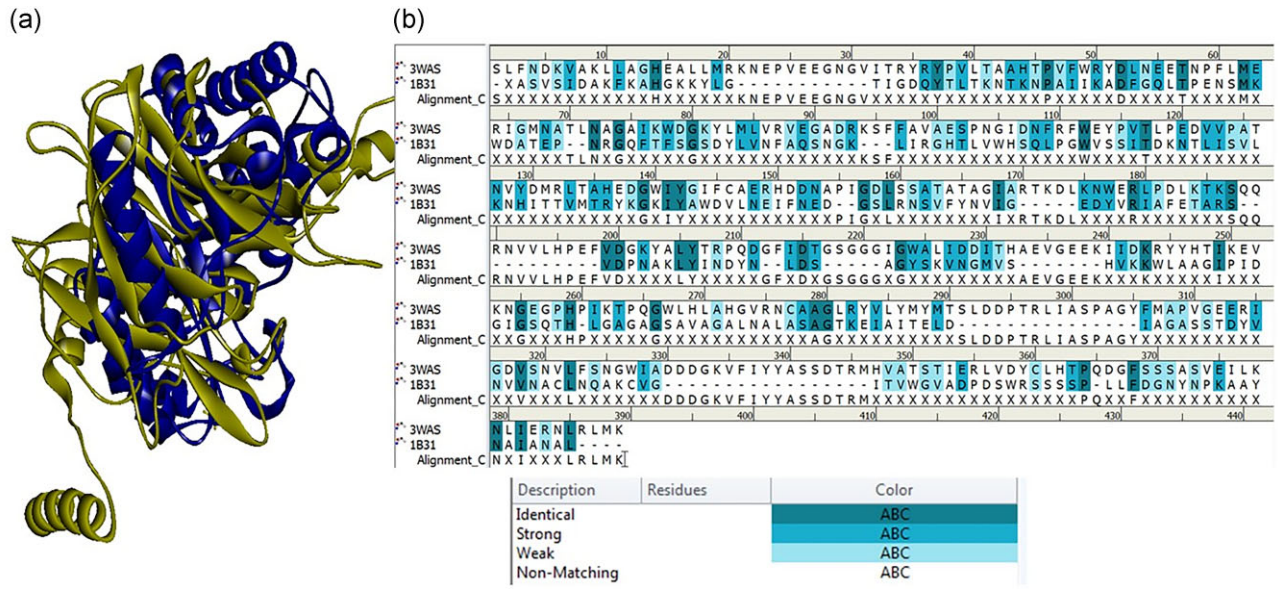

Fig. 5. Comparative analysis of the structure and sequence of AH2 with the reference β-1,4-xylanase (PDB ID: 1B31). (a) Superimposition analysis of AH2 (yellow) and 1B31 (blue) with an RMSD of 19.772 Å, (b) Sequence alignment highlighting conserved regions with residues colored by their conservation grade.

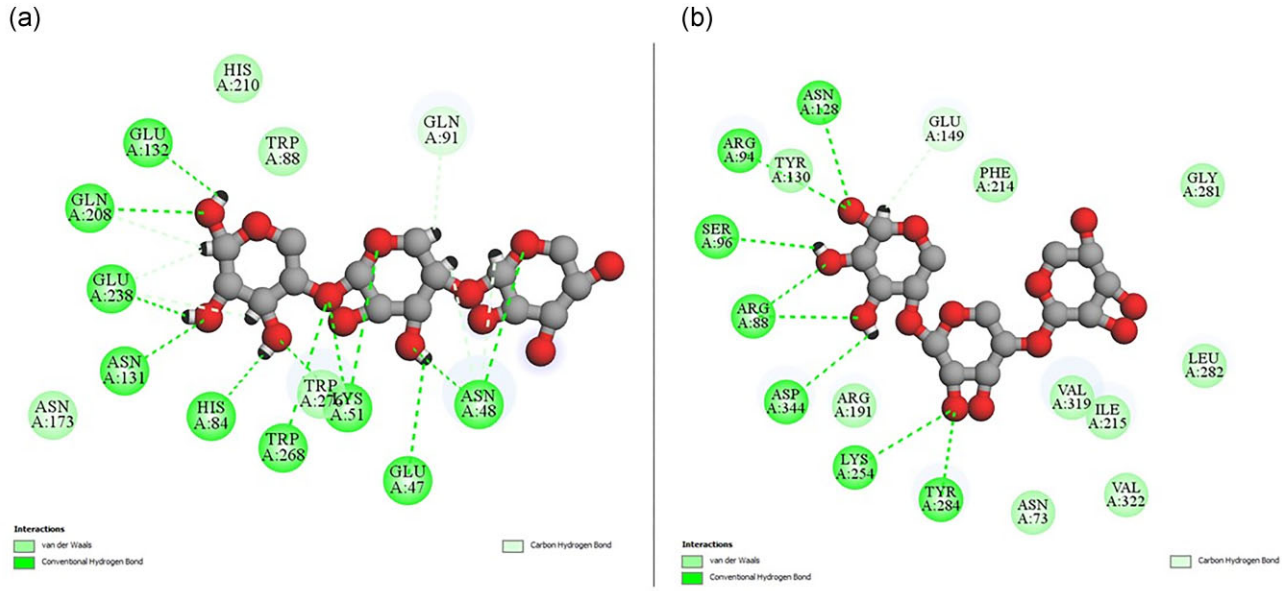

Fig. 6. Interaction diagram of beta-D-xylopyranose-(1–4)-beta-D-xylopyranose (PDB ID: 1B31-substrate) along with, (a) 1B31: 2D interaction diagram and (b) AH2: 2D interaction diagram.

A prior study attempted broader substrate screenings for GH130 enzymes, testing polysaccharides such as xylan (from birchwood), xyloglucan, lichenan, glucomannan, and carboxymethylcellulose (Rosewarne et al., 2014). While some enzymes displayed activity on glucomannan and carboxymethylcellulose, none exhibited xylanase activity, emphasizing that xylanase activity has not been previously associated with GH130 enzymes. However, many GH130 sequences remain biochemically uncharacterized, hence the prospect of discovering additional xylanases within this family is warranted.

Xylanases are versatile enzymes widely used in industries such as biofuel production, chemical manufacturing, animal feed processing, pulp bleaching, and baking, and in laundry detergents, and fabric care products (Kulkarni et al., 1999). Additionally, xylo-oligosaccharides, derived from xylanase-catalyzed hydrolysis of xylan, exhibit prebiotic effects, rendering them valuable additives in beverages and dairy products (Kumar et al., 2018). AH2's exclusive xylanase functionality and the lack of cellulase activity are highly advantageous in industrial applications, as this eliminates the risk of unwanted hydrolysis of cellulose fibers during processing, aligning with the requirements for ideal xylanases in these industries (Subramaniyan & Prema, 2002).

The specific activity of AH2, quantified at 5.5 ± 0.28 U/mg (5500 ± 280 U/g), demonstrates noteworthy competitive potential within the broader context of xylanases from various GH families. This activity is comparable to that of the GH11 xylanase from

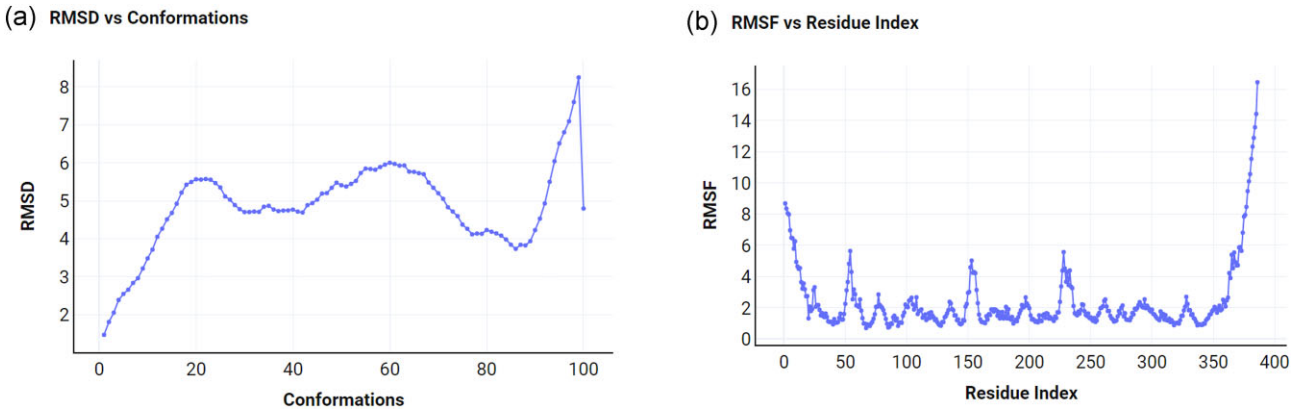

Fig. 7. Structural stability analysis of AH2 (a) RMSD in Å vs. time and (b) RMSF in Å vs. residue index.

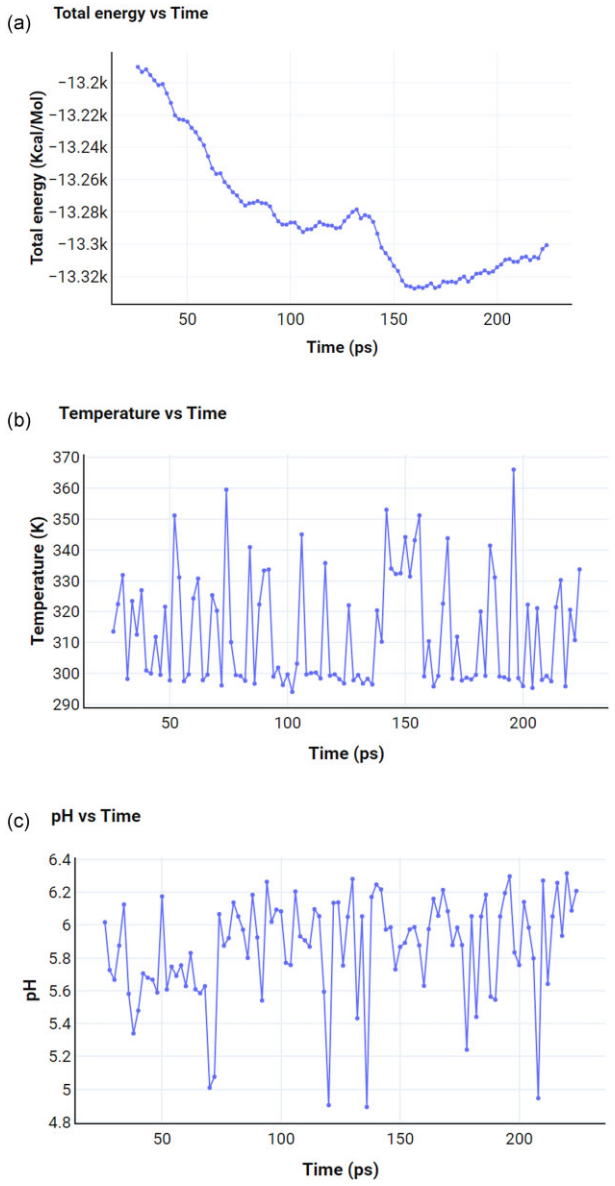

Fig. 8. Stability study of free AH2. (a) Total energy profile. (b) Temperature sensitivity of the AH2's stability, vs. time in 10^{-12} s. (c) pH range in which the AH2 exhibits optimal stability as appeared in the biological results (from 90 to 100%).

Bacillus sp. isolated from termite abdomens, which exhibited a similar specific activity of 5.45 U/mg (Safitri et al., 2021). Additionally, AH2 outperforms other xylanases, including a thermostable recombinant GH11 xylanase from a *Bacillus subtilis* strain isolated from soil (2.2 U/mg) (Saleem et al., 2021) and another recombinant GH11 xylanase from *Bacillus amyloliquefaciens* (2.63 U/mg) (Xu et al., 2016). However, it is important to acknowledge that the specific activity of AH2, while competitive, is lower than some of the highest values reported in the literature. For instance, GH11 xylanases from *Streptomyces lividans* have demonstrated significantly higher activities, with reported values of 60 U/mg and 119.5 U/mg. Similarly, the GH11 xylanase from *Thermobifida fusca* exhibited a higher specific activity of 51 U/mg (Gonçalves et al., 2015). Additionally, it is significantly outperformed by the marine bacterium *Thermoanaerobacterium saccharolyticum* NTOU1 enzyme, which exhibited a specific activity of 15 U/mg (Hung et al., 2011).

The observed resilience of AH2's xylanase activity and stability over a wide pH range underscores its suitability for diverse industries, especially those facing extreme pH conditions. Pulp and paper industries favor the utilization of alkali-active xylanase with stability over a wide pH range. However, poultry feed applications require xylanases to maintain activity within the acidic to neutral pH range prevalent in the gut (Dashtestani et al., 2021). pH stands out as a critical factor influencing enzyme activity by altering the 3D conformation of proteins, potentially leading to denaturation and inactivation (Chen et al., 2016). Notably, AH2 exhibited optimal xylanase activity at pH 5.6 (the computed pI is 5.7); this small difference in optimal pH values may have been caused by not testing 5.7 practically but testing the pH of 5 and 6 where both caused a reduction in activity. Additionally, AH2 had a significant tolerance to a broad pH spectrum (pH 3–9) at 50°C (>70% residual activity). Studies on specific xylanases from diverse sources reveal variability in optimal pH conditions that ranged between 4 and 9 (Gupta et al., 2000; Hu et al., 2008; Khandeparkar & Bhosle, 2007). Xylanases with optimum activity at pH of 5- 6 were reported previously (Chen et al., 2016; Kulkarni et al., 1999); other xylanases that function at higher or lower pH were isolated from diverse microbial species (Dao et al., 2022).

Additionally, AH2's significant activity at pH 10 (68%) underscores its superior adaptability and performance compared to other xylanases. This exceptional alkaline activity is likely due to its elevated arginine (5%) and histidine (4%) content, which are known to enhance enzyme stability and activity in alkaline environments. Previous studies have analyzed the frequency of positively charged amino acid residues and found that alkaline-active

enzymes often have a higher frequency of arginine and histidine (Dubnovitsky et al., 2005; Shirai et al., 2001). Moreover, Mamo et al. (2009) have linked the efficacy of alkaline-active GH10 xylanases from *Bacillus halodurans* to their specific amino acid compositions, particularly the increased presence of basic residues such as arginine and histidine (Mamo et al., 2009). Talens-Perales and colleagues also reported the possible effect of certain catalytic binding domains on the enzymatic activity at different pH and temperatures (Talens-Perales et al., 2020). AH2 retained approximately 49% of its activity at pH 3, indicating significant resilience and functionality under highly acidic conditions. These findings contrast the general characteristics of most microbial xylanases that are optimally active at neutral to slightly acidic pH, which tend to have diminished activity under lower pH levels (Chen et al., 2016; Ghadikolaei et al., 2019).

AH2 exhibited optimal stability at pH 5.6 after one hour at 4°C, while also retaining more than 75% of its enzymatic activity across a broad pH range (3, 7, and 9). Despite a decrease in stability at pH 11, it still maintained 32% residual activity. In comparison, xylanases with wide pH stability have been previously reported (Li et al., 2009; Sinma et al., 2011), while others exhibit stability over narrower ranges (Korkmaz et al., 2017; Li et al., 2006). For example, a xylanase from *Massilia* sp. retained only 10% activity at pH 11 (Xu et al., 2016), highlighting the superior stability of AH2 at extreme pH levels.

Temperature is another important parameter for assessing the industrial utility of enzymes (Zhao et al., 2021). AH2 exhibited optimal activity at 50°C, maintaining 77–86% activity across a wide temperature range (30–70°C). Even at 80°C, AH2 retained 62% activity, indicating significant thermostability. This optimal temperature aligns with previous reports of bacterial xylanases (Irfan et al., 2016; Joshi et al., 2022; Juturu & Wu, 2012). In contrast, many fungal xylanases exhibit optimal activity around 50°C but lose stability above 60°C (Dhaver et al., 2022; Gaspar et al., 1997).

The evaluation of AH2 thermostability further highlights its adaptability across a broad temperature spectrum with >70% of residual activity at 4, 37, and 70°C, with its least stability observed at 25°C (64%). Most xylanases are reported in the literature with narrower thermostability profiles (Joshi et al., 2022; Mitra et al., 2015; Zhang et al., 2012). Thermostable xylanases were reported previously with similar and higher stability periods at 70°C (Ajeje et al., 2021), with few number of xylanases stable at temperatures below 40°C (Bombardi et al., 2024; Raj et al., 2013). Of note, AH2 retained almost 76% of its activity at 4°C. Stability at low temperatures is an important factor to be considered during different enzymatic processes and storage. The significant enhancement in AH2 activity observed at 50°C following one hour of incubation suggests that standing at its optimal temperature may induce favorable structural or conformational changes in the enzyme, consequently amplifying its catalytic efficacy (Fágáin, 1995; Maffucci et al., 2020). This effect was reported previously for xylanases and other CAZymes (Joshi et al., 2022; Santos et al., 2016).

The thermal activity and stability of AH2 across a wide temperature range highlights its flexibility for use in both low and high-temperature industrial processes. Feed processing often takes place at elevated temperatures (Pasamontes et al., 1997). In bread baking, xylanases transform the insoluble hemicellulose in dough into soluble sugars, making the dough light and yielding soft bread (Collins et al., 2005). Additionally, AH2's stability at refrigerated temperatures might be advantageous because it works well at lower temperatures, improving bread quality before baking, making it suitable in food processing, where consistent enzymatic performance is essential for maintaining product quality and extending shelf life (Bommarius & Paye, 2013).

The utilization of xylanases in industrial applications has encountered significant challenges in achieving commercial viability, primarily due to various factors. These include the limited optimal pH range, thermal instability of enzymes, and high production costs associated with enzyme manufacturing (Walia et al., 2013). While some researchers have explored approaches such as genetic engineering (Lu et al., 2017; Xu et al., 2016) or enzyme immobilization (Kapoor & Kuhad, 2007; Kumar et al., 2013; Madakbaş et al., 2013) to enhance the physical properties of naturally produced bacterial xylanases, AH2's inherent stability and activity in its native form offer distinct advantages in eliminating the cost for enzymatic modifications to cope with the characteristics required by different applications.

A phylogenetic analysis was performed to evaluate the similarity between protein sequences of AH2 and the GH130 enzymes available in the CAZy database. The resulting phylogenetic tree reveals that AH2 clusters within a distinct, well-supported clade of GH130 enzymes, emphasizing its close evolutionary ties to other GH130 members. Despite this close relationship, AH2 exhibits xylanase activity, a trait that is rare among GH130 proteins. In contrast, the GH8 and GH11 families, known for their xylanase activity, appear as outgroups and display significant phylogenetic distance from AH2. This distance highlights a notable sequence divergence between AH2 and these xylanase-active families, even though AH2 performs similar enzymatic functions. Thus, while AH2 shares evolutionary connections with GH130 enzymes, its unique xylanase activity and distinct phylogenetic placement illustrate its functional and evolutionary distinctiveness within the GH130 family. This distinctiveness is evident where one of the AH2's closest relatives within the GH130 family (AGH13967.1) does not exhibit activity against beach wood xylan (Rosewarne et al., 2014).

Following the characterization of AH2 and the confirmation of its exclusive xylanase activity, we employed in silico approaches to investigate the possible underlying structural and molecular basis. Protein alignment analysis was performed to predict the potential active sites and residues involved in AH2 xylanase activity by comparing the homology model of AH2 with those of referenced xylanase proteins, available at the protein data bank. The analysis identified the conserved residues between AH2 and these known enzymes. Among the analyzed proteins, endo-β-1,4-xylanase 1B31 displayed the closest structural resemblance to AH2, as indicated by its lowest RMSD value upon superimposition. This strong structural similarity, along with insights from protein interface interaction analysis, led to the selection of 1B31 for further investigation of its binding interactions with AH2. The conserved residues (Asn69-Asn73-Glu90-Arg94-Glu149) identified from AH2's alignment with other xylanase proteins also matched the corresponding residues Glu56-Asn58-Gln75-Lys79-Asn131 in β-1,4-xylanase 1B31. This alignment highlights AH2's potential active site and supports its xylanase activity. These findings are consistent with previous blind docking and binding site predictions, which identified Glu149 as a key residue responsible for the enzyme's activity. Further confirmation came from the interaction analysis of endo-β-1,4-xylanase 1B31 with AH2, which revealed that Arg88, Glu149, and Asp343 are conserved, aligning well with the docking and binding site prediction results. The observed binding pattern between the 1B31 co-crystallized substrate [beta-D-xylopyranose-(1–4)-beta-D-xylopyranose] and AH2 identified Glu149 as involved in hydrogen bond formation with the candidate substrate. The protein alignment of AH2 to other

xylanases identified the same residues as essential amino acids for AH2 function, strongly suggesting that they play a crucial role in the substrate binding and xylanase activity of AH2. Previous studies on different xylanase enzymes confirmed the presence of two glutamate amino acid catalytic residues in the enzyme active site that are responsible for the cleavage of the xylosidic linkage (Kim et al., 2023; Prajapati et al., 2018; Tahir et al., 2002; Wakarchuk et al., 1994). Further studies are therefore required to predict the crystal structure of AH2 and the active residues involved in xylan binding with site-direct mutagenesis experiments to confirm the essentiality of different residues for the xylanase activity.

The BLAST-based homology modeling identified 3WAS, a GH130 family enzyme with mannosidase activity, as the closest match to AH2, sharing 79% sequence identity. However, practical enzymatic assays confirmed that AH2 exhibits xylanase activity instead.

Molecular dynamics simulations were used to validate and confirm the stability of the AH2 protein, with RMSD analysis revealing a well-folded and stable protein structure throughout the simulation. The low average RMSD value (around 6 Å) and the high percentage of conformations with values below 5.5 Å strongly support this observation. This stability is further confirmed by the low RMSF values (<4 Å for most residues), indicating structural rigidity in critical regions of the protein. Additionally, the energy profile further validates the stability, as the observed decrease in energy over time (average range: −13200 to −13320 kcal/mol) suggests the protein adopts energetically favorable and stable conformations, contributing to the overall stability of AH2. The simulations provided valuable insights into the influence of temperature and pH on AH2 stability, which were used to validate and confirm the actual experimental results. The analysis showed that the protein remained stable below 330 K (56.85°C) most of the time, and the pH stability assessment indicated that the protein maintained at least 90% stability at pH 5.6 Notably, the predicted optimal stability range (pH 4.9–6.8) aligns with the experimentally determined peak stability point at pH 5.6. These findings confirm the results observed *in vitro* regarding the effect of pH and temperature on AH2 enzyme activity and stability, providing a solid foundation for future research.

Conclusions

The metagenome of an equine stool sample presents an unexplored source of novel CAZymes, where AH2 enzyme, annotated as a GH130 family member, had an exclusive xylanase activity, a previously uncharacterized activity of the GH130 family. Docking studies of AH2 confirmed the presence of Glu90 and Glu149, the conserved residues critical for xylanase activity. MD simulation demonstrated remarkable enzyme stability across a broad pH range and temperatures, supporting the in vitro characterization results. The enzyme characteristics confirm suitability for different types of industrial applications and exclude the need for costly manipulations required for the enhancement of a specific activity needed in specialized industrial applications. This further highlights the potential for uncovering novel enzymatic functions within unexplored microbial communities and underscores the importance of further research in understanding microbial diversity and enzymatic potential.

Acknowledgments

The authors would like to thank Dr. Moustafa A. TagElDein for his help in collection of the stool sample and extraction of DNA from the collected sample, Department of Microbiology & Immunology, Faculty of Pharmacy, Cairo University. The authors would also like to acknowledge Haley Merrick & Padam Singh for their assistance in enzymatic expression and purification.

Supplementary Material

Supplementary material is available online at *JIMB* (www.academic.oup.com/jimb).

Author Contributions

Amr Ali Hemeda: writing—original draft, methodology, investigation, formal analysis, data curation. Sara Ahmed Zahran: writing—original draft, writing—review & editing, investigation, formal analysis, data curation, supervision. Marwa Ali-Tammam: writing—review & editing, investigation, formal analysis, data curation, supervision. Menna A. Ewida: writing—original draft, writing—review & editing, investigation, formal analysis, Data curation. Mona Tawfik Kashef: writing—review & editing, supervision, conceptualization, data curation. Ayman Samir Yassin: writing—review & editing, supervision, conceptualization, data curation. Avishek Mitra: methodology, formal analysis, data curation, writing—review & editing, supervision. Noha H. Yousef: methodology, formal analysis, data curation, writing—review & editing, supervision funding acquisition. Mostafa S. Elshahed: methodology, formal analysis, data curation, writing—review & editing, supervision, funding acquisition.

Funding

Amr Ali Hemeda has been supported by a scholarship from the United States Agency for International Development (USAID). Part of this work has been funded by the American National Science Foundation (NSF) grant number 2029478 to Mostafa S. Elshahed and Noha H. Youssef, the US National Institute of Health (NIH) grant number P20GM152333 to MSE, and the NIH grant number P20GM134973 to Avishek Mitra.

Conflict of Interest

The authors declare that they have no known competing financial interests or personal relationships that could have appeared to influence the work reported in this paper.

References

Agarwal, G., Mahajan, S., Srinivasan, N., & de Brevern, A. G. (2011). Identification of local conformational similarity in structurally variable regions of homologous proteins using protein blocks. *PLoS One*, *6*(3), e17826. https://doi.org/10.1371/journal.pone.0017826

Ajeje, S. B., Hu, Y., Song, G., Peter, S. B., Afful, R. G., Sun, F., Asadollahi, M. A., Amiri, H., Abdulkhani, A., & Sun, H. (2021). Thermostable cellulases/xylanases from thermophilic and hyperthermophilic microorganisms: Current perspective. *Frontiers in Bioengineering and Biotechnology*, 9, 794304. https://doi.org/10.3389/fbioe.2021.794304

Arkin, A. P., Cottingham, R. W., Henry, C. S., Harris, N. L., Stevens, R. L., Maslov, S., Dehal, P., Ware, D., Perez, F., Canon, S., Sneddon, M. W., Henderson, M. L., Riehl, W. J., Murphy-Olson, D., Chan, S. Y., Kamimura, R. T., Kumari, S., Drake, M. M., Brettin, T. S., & Yu, D. (2018). KBase: The United States Department of Energy Systems

Biology Knowledgebase. *Nature Biotechnology*, 36(7), 566–569. https://doi.org/10.1038/nbt.4163

Aÿ, J., Götz, F., Borriss, R., & Heinemann, U. (1998). Structure and function of the Bacillus hybrid enzyme GluXyn-1: Native-like jellyroll fold preserved after insertion of autonomous globular domain. *Proceedings of the National Academy of Sciences*, 95(12), 6613–6618. https://doi.org/10.1073/pnas.95.12.6613

Bergmann, G. T. (2017). Microbial community composition along the digestive tract in forage- and grain-fed bison. *BMC Veterinary Research*, 13,(1), 253. https://doi.org/10.1186/s12917-017-1161-x

Berlemont, R., & Martiny, A. C. (2015). Genomic potential for polysaccharide deconstruction in bacteria. *Applied and Environmental Microbiology*, 81(4), 1513–1519. https://doi.org/10.1128/AEM.03718-14

Bolger, A. M., Lohse, M., & Usadel, B. (2014). Trimmomatic: A flexible trimmer for Illumina sequence data. *Bioinformatics*, 30(15), 2114–2120. https://doi.org/10.1093/bioinformatics/btu170

Bombardi, L., Salini, A., Aulitto, M., Zuliani, L., Andreolli, M., Bordoli, P., Coltro, A., Vitulo, N., Zaccone, C., Lampis, S., & Fusco, S. (2024). Lignocellulolytic potential of microbial consortia isolated from a local biogas plant: The case of thermostable xylanases secreted by mesophilic bacteria. *International Journal of Molecular Sciences*, 25(2), 1090. https://doi.org/10.3390/ijms25021090

Bommarius, A. S., & Paye, M. F. (2013). Stabilizing biocatalysts. *Chemical Society Reviews*, 42(15), 6534–6565. https://doi.org/10.1039/C3CS60137D

Breuil, C., & Saddler, J. N. (1985). Comparison of the 3,5-dinitrosalicylic acid and Nelson-Somogyi methods of assaying for reducing sugars and determining cellulase activity. *Enzyme and Microbial Technology*, 7(7), 327–332. https://doi.org/10.1016/0141-0229(85)90111-5

Buchfink, B., Reuter, K., & Drost, H.-G. (2021). Sensitive protein alignments at tree-of-life scale using DIAMOND. *Nature Methods*, 18(4), 366–368. https://doi.org/10.1038/s41592-021-01101-x

Cantarel, B. L., Coutinho, P. M., Rancurel, C., Bernard, T., Lombard, V., & Henrissat, B. (2009). The Carbohydrate-Active EnZymes database (CAZy): An expert resource for glycogenomics. *Nucleic Acids Research*, 37(Database), D233–D238. https://doi.org/10.1093/nar/gkn663

Chen, Q., Li, M., & Wang, X. (2016). Enzymology properties of two different xylanases and their impacts on growth performance and intestinal microflora of weaned piglets. *Animal Nutrition*, 2(1), 18–23. https://doi.org/10.1016/j.aninu.2016.02.003

Cholewińska, P., Czyż, K., Nowakowski, P., & Wyrostek, A. (2020). The microbiome of the digestive system of ruminants—A review. *Animal Health Research Reviews*, 21(1), 3–14. https://doi.org/10.1017/S1466252319000069

Collins, T., Gerday, C., & Feller, G. (2005). Xylanases, xylanase families and extremophilic xylanases. *FEMS Microbiology Reviews*, 29(1), 3–23. https://doi.org/10.1016/j.femsre.2004.06.005

Cuskin, F., Baslé, A., Ladevèze, S., Day, A. M., Gilbert, H. J., Davies, G. J., Potocki-Véronèse, G., & Lowe, E. C. (2015). The GH130 family of mannoside phosphorylases contains glycoside hydrolases that target β-1,2-mannosidic linkages in Candida Mannan. *Journal of Biological Chemistry*, 290(41), 25023–25033. https://doi.org/10.1074/jbc.M115.681460

Dao, T. M. A., Cuong, N. T., Nguyen, T. T., Nguyen, N. P. D., & Tuyen, D. T. (2022). Purification, identification, and characterization of a glycoside hydrolase family 11-xylanase with high activity from *Aspergillus niger* VTCC 017. *Molecular Biotechnology*, 64(2), 187–198. https://doi.org/10.1007/s12033-021-00395-8

Dashtestani, F., Ma'mani, L., Jokar, F., Maleki, M., Eskandari Fard, M., & Hosseini Salekdeh, G. (2021). Zeolite-based nanocomposite as a smart pH-sensitive nanovehicle for release of xylanase as poultry feed supplement. *Scientific Reports*, 11,(1), 21386. https://doi.org/10.1038/s41598-021-00688-7

Dhaver, P., Pletschke, B., Sithole, B., & Govinden, R. (2022). Isolation, screening, preliminary optimisation and characterisation of thermostable xylanase production under submerged fermentation by fungi in Durban, South Africa. *Mycology*, 13(4), 271–292. https://doi.org/10.1080/21501203.2022.2079745

Dicks, L. M. T., Botha, M., Dicks, E., & Botes, M. (2014). The equine gastro-intestinal tract: An overview of the microbiota, disease and treatment. *Livestock Science*, 160, 69–81. https://doi.org/10.1016/j.livsci.2013.11.025

Drula, E., Garron, M.-L., Dogan, S., Lombard, V., Henrissat, B., & Terrapon, N. (2022). The carbohydrate-active enzyme database: Functions and literature. *Nucleic Acids Research*, 50(D1), D571–D577. https://doi.org/10.1093/nar/gkab1045

Dubnovitsky, A. P., Kapetaniou, E. G., & Papageorgiou, A. C. (2005). Enzyme adaptation to alkaline pH: Atomic resolution (1.08 Å) structure of phosphoserine aminotransferase from *Bacillus alcalophilus*. *Protein Science*, 14(1), 97–110. https://doi.org/10.1110/ps.041029805

Elhusseiny, S. M., El-Mahdy, T. S., Elleboudy, N. S., Yahia, I. S., Farag, M. M. S., Ismail, N. S. M., Yassien, M. A., & Aboshanab, K. M. (2022). In vitro anti SARS-CoV-2 activity and docking analysis of *Pleurotus ostreatus*, *Lentinula edodes* and *Agaricus bisporus* edible Mushrooms. *Infection and Drug Resistance*, *Volume* 15, 3459–3475. https://doi.org/10.2147/IDR.S362823

Fágáin, C. O. (1995). Understanding and increasing protein stability. *Biochimica et Biophysica Acta (BBA)—Protein Structure and Molecular Enzymology*, 1252(1), 1–14. https://doi.org/10.1016/0167-4838(95)00133-f

Forcina, G., Pérez-Pardal, L., Carvalheira, J., & Beja-Pereira, A. (2022). Gut microbiome studies in livestock: Achievements, challenges, and perspectives. *Animals*, 12(23), 3375. https://doi.org/10.3390/ani12233375

Froger, A., & Hall, J. E. (2007). Transformation of plasmid DNA into E. coli using the heat shock method. *Journal of Visualized Experiments*, 6(6), 253. https://doi.org/10.3791/253

Gaspar, A., Cossch, T., Roques, C., & Thonart, P.h. (1997). Study on the production of a xylanolytic complex from *Penicillium canescens* 10-10c. *Applied Biochemistry and Biotechnology*, 67(1-2), 45–58. https://doi.org/10.1007/BF02787840

Ghadikolaei, K. K., Sangachini, E. D., Vahdatirad, V., Noghabi, K. A., & Zahiri, H. S. (2019). An extreme halophilic xylanase from camel rumen metagenome with elevated catalytic activity in high salt concentrations. *AMB Express*, 9(1), 86. https://doi.org/10.1186/s13568-019-0809-2

Gonçalves, G. A. L., Takasugi, Y., Jia, L., Mori, Y., Noda, S., Tanaka, T., Ichinose, H., & Kamiya, N. (2015). Synergistic effect and application of xylanases as accessory enzymes to enhance the hydrolysis of pretreated bagasse. *Enzyme and Microbial Technology*, 72, 16–24. https://doi.org/10.1016/j.enzmictec.2015.01.007

Gübitz, G. (1999). Xylan binding subsite mapping in the xylanase from *Penicillium simplicissimum* using xylooligosaccharides as cryoprotectant. *Biochemistry*, 38, 2403–2412. https://www.academia.edu/13707040/Xylan_Binding_Subsite_Mapping_in_the_Xylanase_from_Penicillium_simplicissimum_Using_Xylooligosaccharides_as_CryoProtectant

Gupta, S., Bhushan, B., & Hoondal, G. S. (2000). Isolation, purification and characterization of xylanasefrom Staphylococcus sp. SG-13 and its application in biobleaching of kraft pulp. *Journal of Applied Microbiology*, 88(2), 325–334. https://doi.org/10.1046/j.1365-2672.2000.00974.x

Hu, Y., Zhang, G., Li, A., Chen, J., & Ma, L. (2008). Cloning and enzymatic characterization of a xylanase gene from a soil-derived metagenomic library with an efficient approach. *Applied Microbiology and Biotechnology*, *80*(5), 823–830. https://doi.org/10.1007/s00253-008-1636-6

Hung, K.-S., Liu, S.-M., Tzou, W.-S., Lin, F.-P., Pan, C.-L., Fang, T.-Y., Sun, K.-H., & Tang, S.-J. (2011). Characterization of a novel GH10 thermostable, halophilic xylanase from the marine bacterium *Thermoanaerobacterium saccharolyticum* NTOU1. *Process Biochemistry*, *46*(6), 1257–1263. https://doi.org/10.1016/j.procbio.2011.02.009

Irfan, M., Asghar, U., Nadeem, M., Nelofer, R., & Syed, Q. (2016). Optimization of process parameters for xylanase production by *Bacillus* sp. In submerged fermentation. *Journal of Radiation Research and Applied Sciences*, *9*(2), 139–147. https://doi.org/10.1016/j.jrras.2015.10.008

Joshi, J. B., Priyadharshini, R., & Uthandi, S. (2022). Glycosyl hydrolase 11 (xynA) gene with xylanase activity from thermophilic bacteria isolated from thermal springs. *Microbial Cell Factories*, *21*(1), 62. https://doi.org/10.1186/s12934-022-01788-3

Julliand, V., & Grimm, P. (2017). The Impact of Diet on the Hindgut Microbiome. *Journal of Equine Veterinary Science*, *52*, 23–28. https://doi.org/10.1016/j.jevs.2017.03.002

Juturu, V., & Wu, J. C. (2012). Microbial xylanases: Engineering, production and industrial applications. *Biotechnology Advances*, *30*(6), 1219–1227. https://doi.org/10.1016/j.biotechadv.2011.11.006

Kapoor, M., & Kuhad, R. C. (2007). Immobilization of xylanase from Bacillus pumilus strain MK001 and its application in production of xylo-oligosaccharides. *Applied Biochemistry and Biotechnology*, *142*(2), 125–138. https://doi.org/10.1007/s12010-007-0013-8

Karasov, W. H., & Douglas, A. E. (2013). Comparative Digestive Physiology. *Comprehensive Physiology*, *3*(2), 741–783. https://doi.org/10.1002/cphy.c110054

Khandeparkar, R., & Bhosle, N. B. (2007). Application of thermoalkalophilic xylanase from Arthrobacter sp. MTCC 5214 in biobleaching of kraft pulp. *Bioresource Technology*, *98*(4), 897–903. https://doi.org/10.1016/j.biortech.2006.02.037

Kim, I. J., Kim, S. R., Kim, K. H., Bornscheuer, U. T., & Nam, K. H. (2023). Characterization and structural analysis of the endo-1,4-β-xylanase GH11 from the hemicellulose-degrading *Thermoanaerobacterium saccharolyticum* useful for lignocellulose saccharification. *Scientific Reports*, *13*(1), 17332. https://doi.org/10.1038/s41598-023-44495-8

Korkmaz, M. N., Ozdemir, S. C., & Uzel, A. (2017). Xylanase production from marine derived *Trichoderma pleuroticola* 08ÇK001 strain isolated from Mediterranean coastal sediments. *Journal of Basic Microbiology*, *57*(10), 839–851. https://doi.org/10.1002/jobm.201700135

Kulkarni, N., Shendye, A., & Rao, M. (1999). Molecular and biotechnological aspects of xylanases. *FEMS Microbiology Reviews*, *23*(4), 411–456. https://doi.org/10.1111/j.1574-6976.1999.tb00407.x

Kumar, P., Gupta, A., Dhakate, S. R., Mathur, R. B., Nagar, S., & Gupta, V. K. (2013). Covalent immobilization of xylanase produced from *Bacillus pumilus* SV-85S on electrospun polymethyl methacrylate nanofiber membrane. *Biotechnology and Applied Biochemistry*, *60*(2), 162–169. https://doi.org/10.1002/bab.1072

Kumar, V., Dangi, A. K., & Shukla, P. (2018). Engineering thermostable microbial xylanases toward its industrial applications. *Molecular Biotechnology*, *60*(3), 226–235. https://doi.org/10.1007/s12033-018-0059-6

Laemmli, U. K. (1970). Cleavage of structural proteins during the assembly of the head of bacteriophage T4. *Nature*, *227*(5259), 680–685. https://doi.org/10.1038/227680a0

Li, A., Laville, E., Tarquis, L., Lombard, V., Ropartz, D., Terrapon, N., Henrissat, B., Guieysse, D., Esque, J., Durand, J., Morgavi, D. P., & Potocki-Veronese, G. (2020). Analysis of the diversity of the glycoside hydrolase family 130 in mammal gut microbiomes reveals a novel mannoside-phosphorylase function. *Microbial Genomics*, *6*(10), mgen000404. https://doi.org/10.1099/mgen.0.000404

Li, C., Li, X., Guo, R., Ni, W., Liu, K., Liu, Z., Dai, J., Xu, Y., Abduriyim, S., Wu, Z., Zeng, Y., Lei, B., Zhang, Y., Wang, Y., Zeng, W., Zhang, Q., Chen, C., Qiao, J., Liu, C., & Hu, S. (2023). Expanded catalogue of metagenome-assembled genomes reveals resistome characteristics and athletic performance-associated microbes in horse. *Microbiome*, *11*(1), 7. https://doi.org/10.1186/s40168-022-01448-z

Li, D., Liu, C.-M., Luo, R., Sadakane, K., & Lam, T.-W. (2015). MEGAHIT: An ultra-fast single-node solution for large and complex metagenomics assembly via succinct de Bruijn graph. *Bioinformatics*, *31*(10), 1674–1676. https://doi.org/10.1093/bioinformatics/btv033

Li, L., Tian, H., Cheng, Y., Jiang, Z., & Yang, S. (2006). Purification and characterization of a thermostable cellulase-free xylanase from the newly isolated *Paecilomyces themophila*. *Enzyme and Microbial Technology*, *38*(6), 780–787. https://doi.org/10.1016/j.enzmictec.2005.08.007

Li, N., Shi, P., Yang, P., Wang, Y., Luo, H., Bai, Y., Zhou, Z., & Yao, B. (2009). A xylanase with high pH stability from Streptomyces sp. S27 and its carbohydrate-binding module with/without linker-region-truncated versions. *Applied Microbiology and Biotechnology*, *83*(1), 99–107. https://doi.org/10.1007/s00253-008-1810-x

Lu, Y., Fang, C., Wang, Q., Zhou, Y., Zhang, G., & Ma, Y. (2017). Correction: Corrigendum: High-level expression of improved thermostable alkaline xylanase variant in *Pichia pastoris* through codon optimization, multiple gene insertion and high-density fermentation. *Scientific Reports*, *7*(1), 44719. https://doi.org/10.1038/srep44719

Macdonald, S. S., Armstrong, Z., Morgan-Lang, C., Osowiecka, M., Robinson, K., Hallam, S. J., & Withers, S. G. (2019). Development and application of a high-throughput functional metagenomic screen for glycoside phosphorylases. *Cell Chemical Biology*, *26*(7), 1001–1012.e5. https://doi.org/10.1016/j.chembiol.2019.03.017

Madakbaş, S., Danış, Ö., Demir, S., & Kahraman, M. V. (2013). Xylanase immobilization on functionalized polyaniline support by covalent attachment. *Starch—Stärke*, *65*(1-2), 146–150. https://doi.org/10.1002/star.201200104

Madeira, F., Pearce, M., Tivey, A. R. N., Basutkar, P., Lee, J., Edbali, O., Madhusoodanan, N., Kolesnikov, A., & Lopez, R. (2022). Search and sequence analysis tools services from EMBL-EBI in 2022. *Nucleic Acids Research*, 50(W1), W276–W279. https://doi.org/10.1093/nar/gkac240

Maffucci, I., Laage, D., Sterpone, F., & Stirnemann, G. (2020). Thermal adaptation of enzymes: Impacts of conformational shifts on catalytic activation energy and optimum temperature. *Chemistry—A European Journal*, *26*(44), 10045–10056. https://doi.org/10.1002/chem.202001973

Makowska-Grzyska, M., Kim, Y., Maltseva, N., Li, H., Zhou, M., Joachimiak, G., Babnigg, G., & Joachimiak, A. (2014). Protein production for structural genomics using *E. coli* expression. *Methods in Molecular Biology*, *1140*, 89–105. https://doi.org/10.1007/978-1-4939-0354-2_7

Mamo, G., Thunnissen, M., Hatti-Kaul, R., & Mattiasson, B. (2009). An alkaline active xylanase: Insights into mechanisms of high pH catalytic adaptation. *Biochimie*, *91*(9), 1187–1196. https://doi.org/10.1016/j.biochi.2009.06.017

Marchler-Bauer, A., Derbyshire, M. K., Gonzales, N. R., Lu, S., Chitsaz, F., Geer, L. Y., Geer, R. C., He, J., Gwadz, M., Hurwitz, D. I., Lanczycki, C. J., Lu, F., Marchler, G. H., Song, J. S., Thanki, N., Wang, Z.,

Yamashita, R. A., Zhang, D., Zheng, C., & Bryant, S. H. (2015). CDD: NCBI's conserved domain database. *Nucleic Acids Research*, *43*(D1), D222–D226. https://doi.org/10.1093/nar/gku1221

Meili, C. H., Jones, A. L., Arreola, A. X., Habel, J., Pratt, C. J., Hanafy, R. A., Wang, Y., Yassin, A. S., TagElDein, M. A., Moon, C. D., Janssen, P. H., Shrestha, M., Rajbhandari, P., Nagler, M., Vinzelj, J. M., Podmirseg, S. M., Stajich, J. E., Goetsch, A. L., Hayes, J., & Elshahed, M. S. (2023). Patterns and determinants of the global herbivorous mycobiome. *Nature Communications*, *14*(1), 3798. https://doi.org/10.1038/s41467-023-39508-z

Mistry, J., Chuguransky, S., Williams, L., Qureshi, M., Salazar, G. A., Sonnhammer, E. L. L., Tosatto, S. C. E., Paladin, L., Raj, S., Richardson, L. J., Finn, R. D., & Bateman, A. (2021). Pfam: The protein families database in 2021. *Nucleic Acids Research*, *49*(D1), D412–D419. https://doi.org/10.1093/nar/gkaa913

Mitchell, A., Chang, H.-Y., Daugherty, L., Fraser, M., Hunter, S., Lopez, R., McAnulla, C., McMenamin, C., Nuka, G., Pesseat, S., Sangrador-Vegas, A., Scheremetjew, M., Rato, C., Yong, S.-Y., Bateman, A., Punta, M., Attwood, T. K., Sigrist, C. J. A., Redaschi, N., & Finn, R. D. (2015). The InterPro protein families database: The classification resource after 15 years. *Nucleic Acids Research*, *43*(D1), D213–D221. https://doi.org/10.1093/nar/gku1243

Mitra, S., Mukhopadhyay, B. C., Mandal, A. R., Arukha, A. P., Chakrabarty, K., Das, G. K., Chakrabartty, P. K., & Biswas, S. R. (2015). Cloning, overexpression, and characterization of a novel alkali-thermostable xylanase from Geobacillus sp. WBI. *Journal of Basic Microbiology*, 55(4), 527–537. https://doi.org/10.1002/jobm.201400495

Morrison, J. M., Elshahed, M. S., & Youssef, N. (2016). A multifunctional GH39 glycoside hydrolase from the anaerobic gut fungus Orpinomyces sp. Strain C1A. *PeerJ*, 4, e2289. https://doi.org/10.7717/peerj.2289

Nihira, T., Chiku, K., Suzuki, E., Nishimoto, M., Fushinobu, S., Kitaoka, M., Ohtsubo, K., & Nakai, H. (2015). An inverting β-1,2-mannosidase belonging to glycoside hydrolase family 130 from *Dyadobacter fermentans*. *FEBS Letters*, *589*(23), 3604–3610. https://doi.org/10.1016/j.febslet.2015.10.008

Nin-Hill, A., Piniello, B., & Rovira, C. (2023). In silico modelling of the function of disease-related CAZymes. *Essays in Biochemistry*, *67*(3), 355–372. https://doi.org/10.1042/EBC20220218

Nurk, S., Meleshko, D., Korobeynikov, A., & Pevzner, P. A. (2017). metaSPAdes: A new versatile metagenomic assembler. *Genome Research*, *27*(5), 824–834. https://doi.org/10.1101/gr.213959.116

O'Leary, N. A., Wright, M. W., Brister, J. R., Ciufo, S., Haddad, D., McVeigh, R., Rajput, B., Robbertse, B., Smith-White, B., Ako-Adjei, D., Astashyn, A., Badretdin, A., Bao, Y., Blinkova, O., Brover, V., Chetvernin, V., Choi, J., Cox, E., Ermolaeva, O., & Pruitt, K. D. (2016). Reference sequence (RefSeq) database at NCBI: Current status, taxonomic expansion, and functional annotation. *Nucleic Acids Research*, *44*(D1), D733–D745. https://doi.org/10.1093/nar/gkv1189

Pasamontes, L., Haiker, M., Wyss, M., Tessier, M., & van Loon, A. P. (1997). Gene cloning, purification, and characterization of a heat-stable phytase from the fungus *Aspergillus fumigatus*. *Applied and Environmental Microbiology*, *63*(5), 1696–1700. https://doi.org/10.1128/aem.63.5.1696-1700.1997

Peng, Y., Leung, H. C. M., Yiu, S. M., & Chin, F. Y. L. (2012). IDBA-UD: A de novo assembler for single-cell and metagenomic sequencing data with highly uneven depth. *Bioinformatics*, *28*(11), 1420–1428. https://doi.org/10.1093/bioinformatics/bts174

Potter, S. C., Luciani, A., Eddy, S. R., Park, Y., Lopez, R., & Finn, R. D. (2018). HMMER web server: 2018 update. *Nucleic Acids Research*, *46*(W1), W200–W204. https://doi.org/10.1093/nar/gky448

Prajapati, A. S., Pawar, V. A., Panchal, K. J., Sudhir, A. P., Dave, B. R., Patel, D. H., & Subramanian, R. B. (2018). Effects of substrate binding site residue substitutions of xynA from *Bacillus amyloliquefaciens* on substrate specificity. *BMC Biotechnology*, *18*(1), 9. https://doi.org/10.1186/s12896-018-0420-7

Price, M. N., Dehal, P. S., & Arkin, A. P. (2010). FastTree 2–approximately maximum-likelihood trees for large alignments. *PLoS ONE*, *5*(3), e9490. https://doi.org/10.1371/journal.pone.0009490

Raj, A., Kumar, S., & Singh, S. K. (2013). A highly thermostable xylanase from *Stenotrophomonas maltophilia*: Purification and partial characterization. *Enzyme Research*, *2013*, 1. https://doi.org/10.1155/2013/429305

Rosewarne, C. P., Pope, P. B., Cheung, J. L., & Morrison, M. (2014). Analysis of the bovine rumen microbiome reveals a diversity of Sus-like polysaccharide utilization loci from the bacterial phylum Bacteroidetes. *Journal of Industrial Microbiology and Biotechnology*, *41*(3), 601–606. https://doi.org/10.1007/s10295-013-1395-y

Rost, B. (1999). Twilight zone of protein sequence alignments. *Protein Engineering, Design and Selection*, *12*(2), 85–94. https://doi.org/10.1093/protein/12.2.85

Safitri, E., Hanifah, P., Sudarko, N.i N. T. P., Ratnadewi, I., & A., A. (2021). Cloning, purification, and characterization of recombinant endo-β-1,4-D-xylanase of *Bacillus* sp. from soil termite abdomen. *Biocatalysis and Agricultural Biotechnology*, 31, 101877. https://doi.org/10.1016/j.bcab.2020.101877

Sakaguchi, S., Takahashi, S., Sasaki, T., Kumagai, T., & Nagata, K. (2011). Progression of alcoholic and non-alcoholic steatohepatitis: Common metabolic aspects of innate immune system and oxidative stress. *Drug Metabolism and Pharmacokinetics*, *26*(1), 30–46.

Saleem, A., Waris, S., Ahmed, T., & Tabassum, R. (2021). Biochemical characterization and molecular docking of cloned xylanase gene from Bacillus subtilis RTS expressed in *E. coli*. *International Journal of Biological Macromolecules*, *168*, 310–321. https://doi.org/10.1016/j.ijbiomac.2020.12.001

Sankey, N., Merrick, H., Singh, P., Rogers, J., Reddi, A., Hartson, S. D., & Mitra, A. (2023). Role of the *Mycobacterium tuberculosis* ESX-4 secretion system in heme iron utilization and pore formation by PPE proteins. *mSphere.*, *8*(2), e0057322. https://doi.org/10.1128/mspheree.00573-22

Santos, T. C. D., Abreu Filho, G., Brito, A. R. D., Pires, A. J. V., Bonomo, R. C. F., & Franco, M. (2016). Production and characterization of cellulolytic enzymes by *Aspergillus nigeR* and *Rhizopus* sp. by solid state fermentation of prickly pear. *Revista Caatinga*, *29*(1), 222–233. https://doi.org/10.1590/1983-21252016v29n126rc

Shirai, T., Ishida, H., Noda, J., Yamane, T., Ozaki, K., Hakamada, Y., & Ito, S. (2001). Crystal structure of alkaline cellulase K: Insight into the alkaline adaptation of an industrial enzyme1. *Journal of Molecular Biology*, *310*(5), 1079–1087. https://doi.org/10.1006/jmbi.2001.4835

Sinma, K., Khucharoenphaisan, K., Kitpreechavanich, V., & Tokuyama, S. (2011). Purification and characterization of a thermostable xylanase from *Saccharopolyspora pathumthaniensis* S582 isolated from the gut of a termite. *Bioscience, Biotechnology, and Biochemistry*, *75*(10), 1957–1963. https://doi.org/10.1271/bbb.110353

Stewart, R. D., Auffret, M. D., Warr, A., Wiser, A. H., Press, M. O., Langford, K. W., Liachko, I., Snelling, T. J., Dewhurst, R. J., Walker, A. W., Roehe, R., & Watson, M. (2018). Assembly of 913 microbial genomes from metagenomic sequencing of the cow rumen. *Nature Communications*, *9*(1), 870. https://doi.org/10.1038/s41467-018-03317-6

Subramaniyan, S., & Prema, P. (2002). Biotechnology of microbial xylanases: Enzymology, molecular biology, and application. *Critical*

Reviews in Biotechnology, *22*(1), 33–64. https://doi.org/10.1080/07388550290789450

Tahir, T. A., Berrin, J.-G., Flatman, R., Roussel, A., Roepstorff, P., Williamson, G., & Juge, N. (2002). Specific characterization of substrate and inhibitor binding sites of a glycosyl hydrolase family 11 xylanase from *Aspergillus niger*. *Journal of Biological Chemistry*, *277*(46), 44035–44043. https://doi.org/10.1074/jbc.M205657200

Takizawa, S., Asano, R., Fukuda, Y., Feng, M., Baba, Y., Abe, K., Tada, C., & Nakai, Y. (2020). Change of endoglucanase activity and rumen microbial community during biodegradation of cellulose using rumen microbiota. *Frontiers in Microbiology*, *11*, 603818. https://doi.org/10.3389/fmicb.2020.603818

Talens-Perales, D., Sánchez-Torres, P., Marín-Navarro, J., & Polaina, J. (2020). In silico screening and experimental analysis of family GH11 xylanases for applications under conditions of alkaline pH and high temperature. *Biotechnology for Biofuels*, *13*(1), 198. https://doi.org/10.1186/s13068-020-01842-5

Tamura, K., Stecher, G., & Kumar, S. (2021). MEGA11: Molecular evolutionary genetics analysis version 11. *Molecular Biology and Evolution*, *38*(7), 3022–3027. https://doi.org/10.1093/molbev/msab120

Wakarchuk, W. W., Campbell, R. L., Sung, W. L., Davoodi, J., & Yaguchi, M. (1994). Mutational and crystallographic analyses of the active site residues of the *Bacillus circulans* xylanase. *Protein Science*, *3*(3), 467–475. https://doi.org/10.1002/pro.5560030312

Walia, A., Mehta, P., Chauhan, A., & Shirkot, C. K. (2013). Optimization of cellulase-free xylanase production by alkalophilic Cellulosimicrobium sp. CKMX1 in solid-state fermentation of apple pomace using central composite design and response surface methodology. *Annals of Microbiology*, *63*(1), 187–198. https://doi.org/10.1007/s13213-012-0460-5

Watzlawick, H. (2017). Measurement of the galactanase activity of the GanB galactanase protein from *Bacillus subtilis*. *Bio-Protocol*, *7*(7), e2206. https://doi.org/10.21769/BioProtoc.2206

Wu, Y.-W., Simmons, B. A., & Singer, S. W. (2016). MaxBin 2.0: An automated binning algorithm to recover genomes from multiple metagenomic datasets. *Bioinformatics*, *32*(4), 605–607. https://doi.org/10.1093/bioinformatics/btv638

Xiang, L., Lu, Y., Wang, H., Wang, M., & Zhang, G. (2019). Improving the specific activity and pH stability of xylanase XynHBN188A by directed evolution. *Bioresources and Bioprocessing*, *6*(1), 25. https://doi.org/10.1186/s40643-019-0262-8

Xu, B., Dai, L., Li, J., Deng, M., Miao, H., Zhou, J., Mu, Y., Wu, Q., Tang, X., Yang, Y., Ding, J., Han, N., & Huang, Z. (2016). Molecular and biochemical characterization of a novel xylanase from Massilia sp. RBM26 isolated from the feces of *Rhinopithecus bieti*. *Journal of Microbiology and Biotechnology*, *26*(1), 9–19. https://doi.org/10.4014/jmb.1504.04021

Yang, J. K., Yoon, H. J., Ahn, H. J., Lee, B. I., Pedelacq, J.-D., Liong, E. C., Berendzen, J., Laivenieks, M., Vieille, C., Zeikus, G. J., Vocadlo, D. J., Withers, S. G., & Suh, S. W. (2004). Crystal structure of beta-D-xylosidase from *Thermoanaerobacterium saccharolyticum*, a family 39 glycoside hydrolase. *Journal of Molecular Biology*, 335(1), 155–165. https://doi.org/10.1016/j.jmb.2003.10.026

Zerbino, D. R., & Birney, E. (2008). Velvet: Algorithms for de novo short read assembly using de Bruijn graphs. *Genome Research*, *18*(5), 821–829. https://doi.org/10.1101/gr.074492.107

Zhang, F., Chen, J.-J., Ren, W.-Z., Lin, L.-B., Zhou, Y., Zhi, X.-Y., Tang, S.-K., & Li, W.-J. (2012). Cloning, expression, and characterization of an alkaline thermostable GH11 xylanase from *Thermobifida halotolerans* YIM 90462T. *Journal of Industrial Microbiology and Biotechnology*, *39*(8), 1109–1116. https://doi.org/10.1007/s10295-012-1119-8

Zhang, H., Yohe, T., Huang, L., Entwistle, S., Wu, P., Yang, Z., Busk, P. K., Xu, Y., & Yin, Y. (2018). dbCAN2: A meta server for automated carbohydrate-active enzyme annotation. *Nucleic Acids Research*, *46*(W1), W95–W101. https://doi.org/10.1093/nar/gky418

Zhao, F., Yu, C.-M., Sun, H.-N., Zhao, L.-S., Ding, H.-T., Cao, H.-Y., Chen, Y., Qin, Q.-L., Zhang, Y.-Z., Li, P.-Y., & Chen, X.-L. (2023). A novel class of xylanases specifically degrade marine red algal β1,3/1,4-mixed-linkage xylan. *Journal of Biological Chemistry*, *299*(9), 105116. https://doi.org/10.1016/j.jbc.2023.105116

Zhao, Y., Miao, Y., Zhi, F., Pan, Y., Zhang, J., Yang, X., Zhang, J. Z. H., & Zhang, L. (2021). Rational design of pepsin for enhanced thermostability via exploiting the guide of structural weakness on stability. *Frontiers in Physics*, *9*, 755253. https://doi.org/10.3389/fphy.2021.755253

Received: September 24, 2024. **Accepted:** February 25, 2025